PROCEEDINGS B

rspb.royalsocietypublishing.org

Research

Cite this article: Lane SJ, Shishido CM, Moran AL, Tobalske BW, Arango CP, Woods HA. 2017 Upper limits to body size imposed by respiratory–structural trade-offs in Antarctic pycnogonids. *Proc. R. Soc. B* **284**: 20171779. http://dx.doi.org/10.1098/rspb.2017.1779

Received: 8 August 2017
Accepted: 26 September 2017

Subject Category:
Ecology

Subject Areas:
ecology

Keywords:
allometry, rate of diffusion, metabolism, pycnogonids, oxygen

Author for correspondence:
Steven J. Lane
e-mail: steven.lane@umontana.edu

Electronic supplementary material is available online at https://dx.doi.org/10.6084/m9.figshare.c.3899374.

THE ROYAL SOCIETY PUBLISHING

Upper limits to body size imposed by respiratory–structural trade-offs in Antarctic pycnogonids

Steven J. Lane[1], Caitlin M. Shishido[2], Amy L. Moran[2], Bret W. Tobalske[1], Claudia P. Arango[3] and H. Arthur Woods[1]

[1]Division of Biological Sciences, University of Montana, Missoula, MT 59812, USA
[2]Department of Biology, University of Hawai'i at Mānoa, Honolulu, HI 96822, USA
[3]Biodiversity Program, Queensland Museum, South Brisbane, Queensland 4101, Australia

SJL, 0000-0002-3361-2244; BWT, 0000-0002-5739-6099; CPA, 0000-0003-1098-830X

Across metazoa, surfaces for respiratory gas exchange are diverse, and the size of those surfaces scales with body size. In vertebrates with lungs and gills, surface area and thickness of the respiratory barrier set upper limits to rates of metabolism. Conversely, some organisms and life stages rely on cutaneous respiration, where the respiratory surface (skin, cuticle, eggshell) serves two primary functions: gas exchange and structural support. The surface must be thin and porous enough to transport gases but strong enough to withstand external forces. Here, we measured the scaling of surface area and cuticle thickness in Antarctic pycnogonids, a group that relies on cutaneous respiration. Surface area and cuticle thickness scaled isometrically, which may reflect the dual roles of cuticle in gas exchange and structural support. Unlike in vertebrates, the combined scaling of these variables did not match the scaling of metabolism. To resolve this mismatch, larger pycnogonids maintain steeper oxygen gradients and higher effective diffusion coefficients of oxygen in the cuticle. Interactions among scaling components lead to hard upper limits in body size, which pycnogonids could evade only with some other evolutionary innovation in how they exchange gases.

1. Background

Understanding how and why rates of oxygen consumption scale with body size is a critical question in integrative biology [1,2]—because body size and metabolic rate play such central roles in physiology, ecology and evolution. One approach to understanding the scaling of organismal traits is to examine how they emerge from the scaling of, and interactions among, lower-level traits [3]. Here we do so for a form of respiratory exchange widely used by aquatic and marine organisms (cnidarians, nemerteans, poriferans, plethodontid salamanders, etc.)—cutaneous gas exchange. This mode is readily modelled using the Fick equation [4], which describes the flux of oxygen across a barrier and, as we describe below, provides a simple, powerful framework for integrating the lower-level traits that influence rates of gas exchange. We examine this problem using sea spiders (Pycnogonida), a diverse and basal clade of arthropods. Our results indicate that respiratory–structural trade-offs play critical roles in the evolution of gas exchange across body sizes. In addition, the scaling of the underlying Fick components suggests physiological limits to upper body size in sea spiders. While most marine arthropods possess specialized respiratory structures, which help them minimize or negate respiratory constraints on their cuticle, sea spiders rely exclusively on cutaneous gas exchange [5], yet still span a wide range of body sizes. Large-bodied individuals may face particularly difficult trade-offs, as their cuticle must withstand external forces while permitting sufficient gas exchange.

In all animals, oxygen moves across respiratory barriers by diffusion, which can be modelled using Fick's law [4,6]. Fick's law states that the flux of oxygen (J, $\mu mol\ s^{-1}$) across a barrier depends on the barrier's conductance (G, $\mu mol\ s^{-1}\ kPa^{-1}$) and the driving gradient for oxygen transport across it

(specifically, the gradient in partial pressure, ΔPO_2, kPa) [7]:

$$J = G \times \Delta PO_2. \quad (1.1)$$

Conductance is thus a measure of how rapidly oxygen moves across a material given a difference in partial pressures. Whole-animal conductance is proportional to the surface area of the respiratory barrier (A, cm^2), the diffusion coefficient of oxygen in the material (D_c, $cm^2\ s^{-1}$), the capacitance coefficient of the medium (β, $\mu mol\ cm^{-3}\ kPa^{-1}$) and it is inversely proportional to the barrier's thickness (x, cm) [7]:

$$G = \frac{A}{x} \times D_c \times \beta. \quad (1.2)$$

The capacitance coefficient describes the increase in oxygen concentration per unit increase in partial pressure [7]. The capacitance coefficient is governed by physical properties and varies based on type of medium (i.e. air, freshwater, saltwater) and temperature of the medium. Substituting equation (1.2) into equation (1.1) gives the flux of oxygen as:

$$J = \frac{A}{x} \times D_c \times \beta \times \Delta PO_2. \quad (1.3)$$

To sustain aerobic metabolism, the flux of oxygen must on average match its consumption by metabolism. If the metabolic rate rises transiently higher than the flux, then internal PO_2 will decline. When internal PO_2 declines too severely, metabolic rate will subsequently decline or the animal must switch over to anaerobic processes. Alternatively, if the metabolic rate falls below the flux, then internal PO_2 will increase. The ΔPO_2 between organism and environment will then decrease, until the flux once again balances the metabolic rate.

The relationship between oxygen flux and metabolic rate in vertebrates, including both endotherms and ectotherms, was recently analysed by Gillooly *et al*. [8]. They examined the size-scaling of both oxygen consumption and oxygen flux, which they defined as diffusive transport of oxygen across respiratory barriers (gills and lungs). Relationships between body mass and respiratory variables are typically described by the power law $Y = aM^b$, where Y is a respiratory variable, M is body mass, a is the normalization constant and b is the scaling exponent [9,10]. The scaling of oxygen consumption in endotherms and ectotherms ($b = 0.75$ and 0.84, respectively) was closely matched by the scaling of diffusive oxygen flux ($b = 0.79$ and 0.82, respectively) [8]. In addition, the 30-fold higher rates of oxygen consumption by endotherms were accommodated by 30-fold higher rates of flux, indicating differences in the normalization constant a [8].

These findings allowed Gillooly *et al*. [8] to estimate how the scaling of oxygen flux emerges from the underlying Fick components. Gillooly *et al*. simplified this problem by leveraging prior results showing that D_c, β and ΔPO_2 are independent of body size ($b = 0$) [11,12], leaving just respiratory barrier thickness (x) and respiratory surface area (A) as potential controls on overall flux. In both endotherms and ectotherms, thickness scaled with a low coefficient ($b = 0.1$ and $b = -0.04$, respectively) and surface area with a high coefficient ($b = 0.89$ and $b = 0.78$, respectively), such that A/x scaled as $b = 0.79$ and $b = 0.82$, respectively, very close to the observed scaling exponents of metabolic rate. Whether the conclusion, that respiratory surface area and barrier thickness entirely explain the scaling of flux, is broadly applicable across animals is unknown. In contrast to most vertebrates, which possess respiratory organs (gills and lungs) whose central function is gas exchange, many animals, particularly marine invertebrates, exchange gases directly across their cuticle or skin, a process called cutaneous gas exchange or 'skin-breathing', or across the eggshells in many egg-laying animals [13,14]. In cutaneous respiration, the cuticle or eggshell must allow adequate gas exchange while still providing structural support, and there is an apparent trade-off between these demands. The surface must be thin or porous enough to permit the diffusion of gases, and the cuticle or eggshell must protect the animal from predators and pathogens, and provide structural resistance to external forces [15–17]. This trade-off has also been hypothesized to exist in vertebrates, as the respiratory barrier must allow gas exchange but also be strong enough to prevent damage from different physical stresses (e.g. changes in gas pressure or surface tension) [6]. However, these internal barriers generally do not experience forces that are as large or as rapidly applied as those experienced by external structures (e.g. high current, grasping predators, crushing forces) and the trade-off may therefore not be as severe.

The conflicting demands of skin-breathing may fundamentally change how the components of Fick's law scale with body size. Perhaps the best-studied example of cutaneous respiration is that of vertebrate and invertebrate eggs. In eggs of most species, oxygen diffuses through air-filled pores in the eggshell [15,18,19]. Eggshell thickness and surface area scale ($b = 0.46$ and 0.66, respectively) with mass [20,21]. These scaling coefficients differ from those found by Gillooly *et al*. [8] for the scaling of respiratory surface area and barrier thickness in vertebrates, probably reflecting that eggshells both exchange gases and provide structural support. In further contrast to adult vertebrates, the combined scaling of eggshell surface area and thickness is insufficient to explain the scaling of avian embryonic metabolism ($b = 0.73$) [22]. To meet this mismatch, pore area scales hypermetrically ($b = 1.24$) [20]. A high scaling coefficient of pore area is effectively similar to a high scaling coefficient of the effective diffusion coefficient (D, equation (1.3)), as a greater pore area allows for greater diffusion of oxygen by increasing the air-filled spaces in which oxygen can move easily. Therefore, an increase in pore surface area helps offset thicker shells and permits the higher oxygen conductance needed to meet the metabolic demands of larger embryos [9,20].

Here we use Antarctic sea spiders (class Pycnogonida) (figure 1), a group of arthropods that rely entirely on cutaneous respiration, to test whether the scaling of metabolic oxygen flux is controlled by just surface area and thickness (electronic supplementary material, figure S1*a*) or by simultaneous scaling of some or all the remaining Fick parameters. Sea spiders lack specialized respiratory structures such as gills, and rely instead on trans-cuticular diffusion of oxygen, probably via pores [5,23]. Like eggshells, the structure of pycnogonid cuticle reflects an evolutionary and functional compromise between gas exchange and structural support: the cuticle must be porous enough to allow in sufficient oxygen but strong enough to prevent buckling. Within the constraints of this trade-off, how do pycnogonids match flux capacity to metabolic rate across body sizes? Body sizes of Antarctic pycnogonids range from approximately 1 cm to approximately 70 cm across all lineages [5]. We envision multiple alternatives that could achieve this matching (electronic supplementary material, figure S1). We limit the full range of possibilities by first characterizing the size-dependence of the two parameters, A and x, that are most likely to be constrained. Because the shape of sea spiders does not change radically with size, we

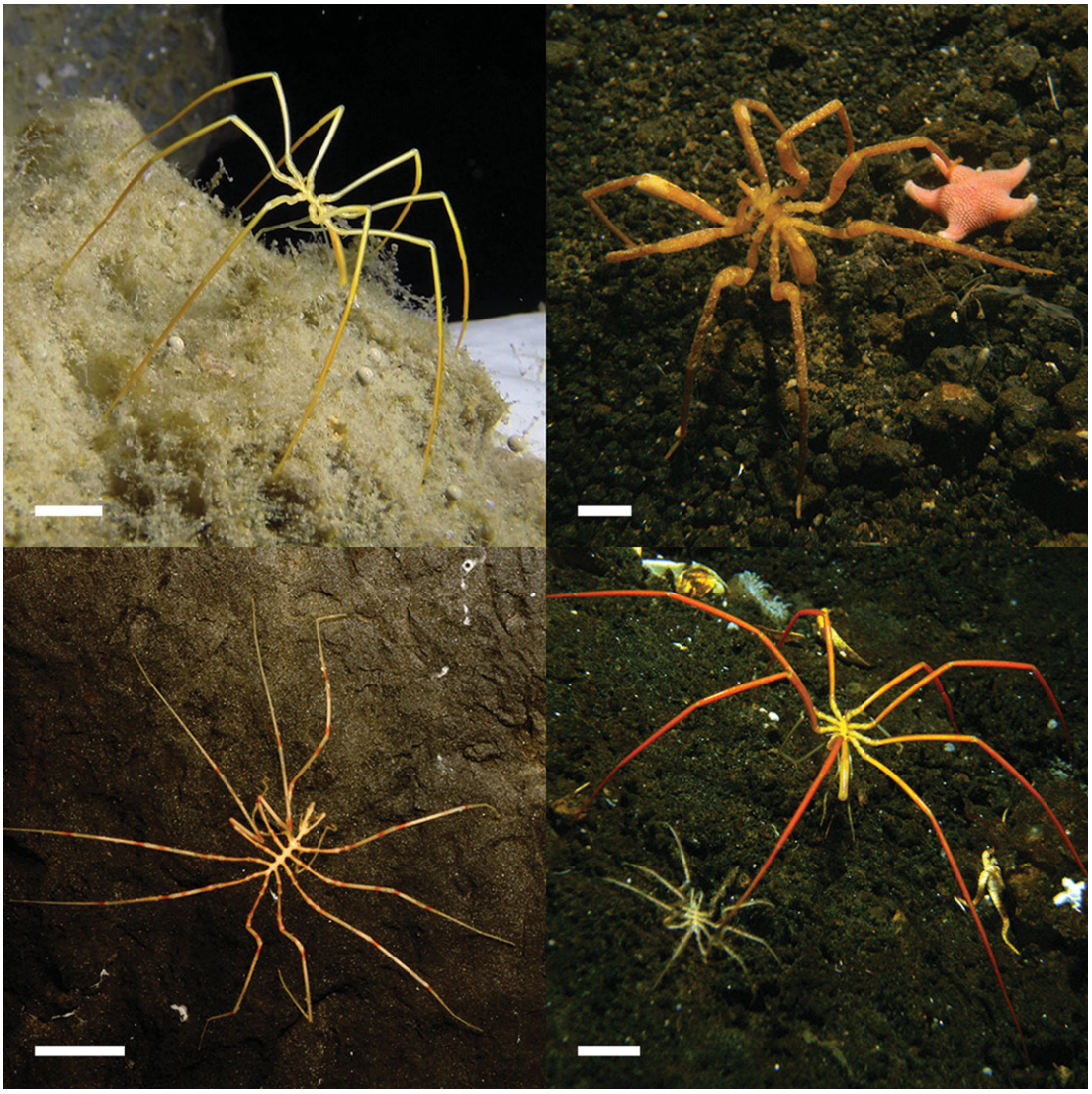

Figure 1. Various sea spiders (Arthropoda, Pycnogonida) collected in McMurdo Sound, Antarctica. Scale bars are approximately 1 cm in each panel. Top left: *Colossendeis megalonyx*, top right: *Ammothea glacialis*, bottom left: *Pentanymphon antarcticum*, bottom right: *Nymphon australe* (smaller animal) and *Colossendeis hoeki* (larger animal). Photo credit to H.A.W. and B.W.T.

expect that A scales with geometric isometry ($b = 0.66$). This prediction is supported by an earlier study of Antarctic sea spiders [24]. We also predict that cuticle thickness, x, scales with geometric isometry ($b = 0.33$), because larger-bodied individuals will need more reinforced legs to handle larger forces. (Note that this is the key point of divergence from thickness of vertebrate respiratory surface, $b = 0.1$ [8].) If the structural variables scale this way, then A/x scales as $b = 0.66 - 0.33 = 0.33$, which is far lower than any expected scaling of metabolic rate. Electronic supplementary material, figure S1*b–d* lays out alternative ways that sea spiders could make up the difference.

In addition to measuring the scaling of oxygen consumption, we also measured the scaling of surface area, cuticle thickness, oxygen gradient across the cuticle and the functional diffusion coefficient of oxygen through sea spider cuticle, which allowed us to estimate the total flux of oxygen across cuticle (using a derivative of Fick's law, equation (1.3)). These factors were measured in 12 species of Pycnogonida from five families.

2. Methods

Sea spiders were collected by diving using SCUBA in McMurdo Sound, Antarctica (77°85′ S, 166°84′ E) in October and November 2015 and 2016. Seawater temperatures averaged −1.8°C. Animals were kept in seawater tables 1–2°C above ambient seawater temperatures and used within two weeks of collection.

Scaling analyses were conducted on 12 Antarctic species (electronic supplementary material, tables S1–S3). Species representatives were identified on the basis of morphology and confirmed using DNA barcoding and published sequences. We used the DNeasy kit (Qiagen, Inc., Valencia, CA, USA) to extract DNA from an approximately 1 mm^3 piece of the dactyl of one leg of each individual pycnogonid. Samples were incubated overnight with 5 µl of proteinase K in a heated (56°C) shaking block (900 r.p.m.). Seven hundred and twelve base pairs of the mitochondrial cytochrome oxidase-1 (*CO1*) gene were PCR-amplified from the extracted DNA using the jgHCO2198 and jgLCO1490 primers of [25]. Reactions were composed of 9.5 µl dH_2O, 12.5 µl *Taq* 2X Ready Mix (Bioline, Taunton, MA, USA), 1 µl of each 10 µM primer and 1 µl of genomic DNA. The amplification cycle consisted of an initial denaturing step at 94°C for 1 m, followed by 30 cycles of 94°C for 1 m, 48°C for 1 m and 72°C for 1 m. PCR products were cleaned by incubating with exonuclease I and shrimp alkaline phosphatase (New England BioLabs, Ipswich, MA, USA) at 37°C for 30 m. Approximately 600–650 bp were then sequenced from each primer by Sanger sequencing at the Advanced Studies in Genomics, Proteomics, and Bioinformatics core facility, University of Hawai'i at Mānoa. Complementary sequences were aligned in Geneious 9.1.5 (Biomatters Ltd., Auckland, NZ). Each consensus sequence was

compared with available GenBank sequences using the BLASTN search routine implemented with default parameters in GenBank.

(a) Oxygen consumption

Rates of oxygen consumption were measured using an oxygen optode system (2-channel FireSting, PyroScience) with temperature-compensation and closed-system respirometry. Chambers were custom-milled from blocks of nylon. Chambers were built in pairs whose volumes were matched to the size of each sea spider measured (9, 17, 70, 292 and 3650 ml; all volumes measured gravimetrically as the difference between mass with and without freshwater), and each chamber had a Teflon-covered magnetic stir bar, shielded with a small housing made of PVC and Nitex mesh to protect the sea spider. During runs, the chambers were held in 5-l baths of water set on top of magnetic stir plates. Initial dye tests showed that water in the chambers was fully mixed in 20–30 s. The sensor spot of the optode system was fixed with silicone glue to thin (less than 2 mm) glass discs, which were sealed to the tops of the chambers with rubber gaskets and held in place with screw-down Plexiglas tops.

Metabolic measurements were made in a cold room with mean temperature −1.1°C (range −1.7 to −0.6°C). In most runs (35 of 38), the chambers were run in pairs, with one blank and the other containing a sea spider. To set up a run, fresh seawater was bubbled with air in the cold room for 6–12 h. Optodes were calibrated at the beginning of every run by immersing them for 5–10 min in the bubbled water and recording the air saturated raw values from both sensors. The bubbles were then turned off and the chambers loaded entirely underwater with its stir bar, housing, and a sea spider (for one of the pair; the other of the pair was identical but contained no sea spider). The chamber was then sealed with the glass disc and Plexiglas top, connected to the fibre optic cable from the optode electronics, and immersed into a water bath on one of the stir plates. The room was dark during respirometry runs. Oxygen levels in the chambers were recorded onto a computer at 1 Hz for 8–24 h using FireSting recording software. Oxygen traces were analysed using scripts written in R (v. 3.0.2) [26]. Using the calibration values, raw sensor values were converted to oxygen concentrations, and the rates of oxygen consumption were estimated by multiplying the volume of the chamber by the difference between the slopes of the traces in the experimental and blank chambers, giving metabolic rate in μmol O_2 h^{-1}. Blank chambers had slopes near zero, indicating little exchange of oxygen between the water and the nylon of the chambers and little consumption of oxygen by microorganisms in the seawater.

(b) Morphological parameters

We measured sea spider body size by weighing and photographing each individual. Individuals were blotted dry and weighed using a microbalance (±0.001 g, AE163 Mettler-Toledo). Sea spiders were photographed (dorsal side) using a stereomicroscope fitted with a Nikon D7100 digital camera and microscope adapter. Individuals too large to be adequately viewed under a stereomicroscope were imaged with the Nikon camera attached to a tripod. Surface area measurements were made in imageJ (v1.49) [27]. Projected surface area for one side was multiplied by two to account for the dorsal and ventral sides. Leg span was also measured in imageJ from these images. Leg span was measured between the tips of the first pair of walking legs as described previously [28]. If one of the legs was damaged or missing, leg span was measured between the second pair of walking legs.

Cuticle thickness was measured on the femur of the second left leg of each individual or, if it was damaged or missing, on the second right leg. The leg was removed from the body and multiple thin sections (less than 1 mm, each) were made of the femur using a single-edge razor blade. Thin sections were cut after measuring diffusion through the leg (see *Diffusion coefficients* below), cross-sectional images were then taken using a compound microscope and cuticle thickness was measured in imageJ.

(c) Oxygen microelectrodes

In the following sections (*Diffusion coefficients* and *Internal oxygen levels*), oxygen levels were measured using Clark-style microelectrodes (50 or 100 μm glass tips; Unisense, Denmark) mounted on a micromanipulator. The electrode was connected to a picoammeter (PA2000; Unisense) and data were recorded once per second by a UI-2 interface (Sable Systems, Las Vegas, NV, USA) controlled by Expedata (v1.8.4; Sable Systems). At the beginning of a set of measurements, an electrode was calibrated at the measurement temperature (between −1.5 and 2°C) using air-bubbled and N_2-bubbled seawater held in a small, water-jacketed glass platform whose temperature was controlled by a recirculating water bath. Between each sea spider the electrode was re-calibrated in air-bubbled seawater.

(d) Diffusion coefficients

The functional diffusion coefficient of oxygen through cuticle reflects two separate diffusion processes: the movement of oxygen directly through the cuticle and the movement of oxygen through tissue-filled pores in the cuticle. Owing to the chitinous exoskeleton of sea spiders, the diffusion of oxygen through cuticle is probably very low, while the diffusion of oxygen through pores is probably very high, close to that of seawater. Therefore, the measured *functional* diffusion coefficients presented here reflect both processes and probably are dominated by diffusion via pores.

We estimated functional diffusion coefficients of oxygen in cuticle using step-change experiments in which oxygen levels inside legs were monitored as external PO_2 was altered [29]. Each measurement was conducted on a single femur from each individual and the step-change took place within the water-jacketed glass platform described above. First, an oxygen electrode was inserted into the centre of a sea spider femur. Once the oxygen electrode within the femur had stabilized, the air-saturated water around the femur was rapidly replaced by deoxygenated (N_2-bubbled) water (generally within 5 s). The container was covered and N_2 gas was bubbled into the container after the step-change to prevent invasion of external O_2. During the step-change, we measured how long it took the internal oxygen pressure to reach zero. This change in oxygen pressure over time was modelled by an analytic equation to estimate the diffusion coefficient of the cuticle [29,30]. We included two layers in the model, the thickness of the cuticle and the radius of the haemocoel. Assumptions of the model included that the electrode was in the centre of the femur and not against the internal cuticle and there was no metabolic consumption of oxygen. The model also assumed that the fluid within the haemocoel was unmixed and that oxygen moved only by diffusion (with a diffusion coefficient identical to that in seawater). Individual runs often took less than 45 min.

To prevent oxygen consumption by leg sections, internal tissues were removed with forceps (in individuals >1 g) or killed using a brief ethanol treatment (in individuals <1 g); additional tests showed that there was no difference in diffusion coefficients in sea spider legs before and after a 2-min treatment with 95% ethanol ($t_7 = 0.689$, $p = 0.513$). In either method, the interior space of the femur was fully filled with seawater before the step-change assay. In large sea spiders (more than 5 g), the femur was sealed from the open environment with Loctite marine epoxy (Henkel Corp., Düsseldorf, Germany) on each end. In small sea spiders (less than 5 g), the oxygen electrode was inserted through the coxa and into the femur, creating a natural seal that prevented the free movement of seawater into the femur. In each case, the femur was held in place in a glass container containing seawater that was bubbled continuously with air.

Table 1. Summary of OLS and PGLS regression analyses for *A* (surface area), *x* (cuticle thickness), D_c (diffusion coefficient), ΔPO_2 (oxygen gradient), *J* (flux), *MR* (metabolic rate) and *LS* (leg span) versus body mass in sea spiders. '*N*' represents number of species used in each analysis. '*a*' represents the intercept and '*b*' represents the scaling exponent. 'mtCO1' indicates PGLS using tree built with unconstrained topology, 'var. brlens' indicates PGLS using tree with variable branch lengths and 'equal brlens' indicates PGLS using same tree topology but with all branch lengths set to 1. Data are listed in electronic supplementary material, tables S1–S3.

models	*N*	*a*	95% CI	*p*	*b*	95% CI	*p*	R^2
A (cm^2); figure 2*a*								
OLS	12	1.15	(1.08,1.21)	<0.001	0.63	(0.54,0.71)	<0.001	0.96
PGLS-mtCO1	12	1.12	(0.95,1.29)	<0.001	0.59	(0.48,0.69)	<0.001	
PGLS-var. brlens	12	1.12	(0.99,1.24)	<0.001	0.58	(0.48,0.69)	<0.001	
PGLS-equal brlens	12	1.13	(0.97,1.28)	<0.001	0.61	(0.50,0.71)	<0.001	
x (cm); figure 2*b*								
OLS	12	−2.22	(−2.37, −2.05)	<0.001	0.27	(0.06,0.49)	0.019	0.38
PGLS-mtCO1	12	−2.32	(−2.70, −1.94)	<0.001	0.15	(−0.09,0.38)	0.196	
PGLS-var. brlens	12	−2.24	(−2.53, −1.95)	<0.001	0.16	(−0.09,0.40)	0.188	
PGLS-equal brlens	12	−2.19	(−2.51, −1.87)	<0.001	0.14	(−0.07,0.36)	0.174	
D_c ($cm^2\ s^{-1}$); figure 2*c*								
OLS	11	−5.93	(−6.05, −5.80)	<0.001	0.20	(0.04,0.37)	0.021	0.40
PGLS-mtCO1	11	−5.96	(−6.27, −5.65)	<0.001	0.12	(−0.12,0.36)	0.300	
PGLS-var. brlens	11	−5.96	(−6.27, −5.65)	<0.001	0.10	(−0.15,0.35)	0.400	
PGLS-equal brlens	11	−5.94	(−6.27, −5.62)	<0.001	0.13	(−0.08,0.35)	0.200	
ΔPO_2 (kPa); figure 2*d*								
OLS	11	0.66	(0.55,0.77)	<0.001	0.27	(0.12,0.42)	0.003	0.60
PGLS-mtCO1	11	0.66	(0.31,1.00)	0.002	0.22	(0.01,0.44)	0.044	
PGLS-var. brlens	11	0.66	(0.41,0.91)	<0.001	0.21	(−0.01,0.44)	0.055	
PGLS-equal brlens	11	0.67	(0.36,0.98)	<0.001	0.19	(−0.02,0.40)	0.069	
J ($\mu mol\ s^{-1}$); figure 3								
OLS	11	−3.71	(−4.06, −3.36)	<0.001	0.83	(0.34,1.31)	0.004	0.58
PGLS-mtCO1	11	−4.01	(−4.83, −3.19)	<0.001	0.64	(0.13,1.15)	0.019	
PGLS-var. brlens	11	−3.89	(−4.53, −3.25)	<0.001	0.65	(0.10,1.20)	0.025	
PGLS-equal brlens	11	−3.77	(−4.65, −2.90)	<0.001	0.74	(0.15,1.34)	0.020	
MR ($\mu mol\ s^{-1}$); figure 3								
OLS	10	−3.96	(−4.15, −3.77)	<0.001	0.80	(0.52,1.08)	0.002	0.83
PGLS-mtCO1	10	−4.03	(−4.47, −3.59)	<0.001	0.77	(0.47,1.08)	<0.001	
PGLS-var. brlens	10	−4.01	(−4.34, −3.69)	<0.001	0.77	(0.47,1.07)	<0.001	
PGLS-equal brlens	10	−3.99	(−4.39, −3.60)	<0.001	0.75	(0.47,1.04)	<0.001	
LS (cm); electronic supplementary material, figure S1								
OLS	12	1.05	(0.97,1.13)	<0.001	0.32	(0.22,0.42)	<0.001	0.81
PGLS-mtCO1	12	1.03	(0.84,1.23)	<0.001	0.27	(0.15,0.39)	<0.001	
PGLS-var. brlens	12	1.02	(0.87,1.16)	<0.001	0.27	(0.15,0.39)	<0.001	
PGLS-equal brlens	12	1.02	(0.83,1.21)	<0.001	0.30	(0.17,0.42)	<0.001	

(e) Internal oxygen levels

On each sea spider, oxygen levels were measured in the femur and in the ambient seawater in which it was contained. A single leg was cut off (underwater) across the second coxa of a living sea spider and the electrode tip was advanced through the third coxa and well into the femur. This process was done as quickly as possible (usually less than 1 min) to minimize changes in internal PO_2 occurring from tissue dead or changes in circulation; this time course is reasonable because metabolic rates are very low. During these measurements, which took several minutes to stabilize for each individual, the temperature of the water in the plastic container generally rose by 1–2°C. The effects of these temperature changes on the electrode readings were offset by noting the local change (rise) in the measured oxygen level in the ambient seawater. Raw electrode readings were converted to oxygen concentrations using the calibration measurements.

(f) Oxygen flux

After estimating the diffusion coefficient of the cuticle (D_c) and measuring the cuticle thickness (*x*), surface area (*S*) and oxygen

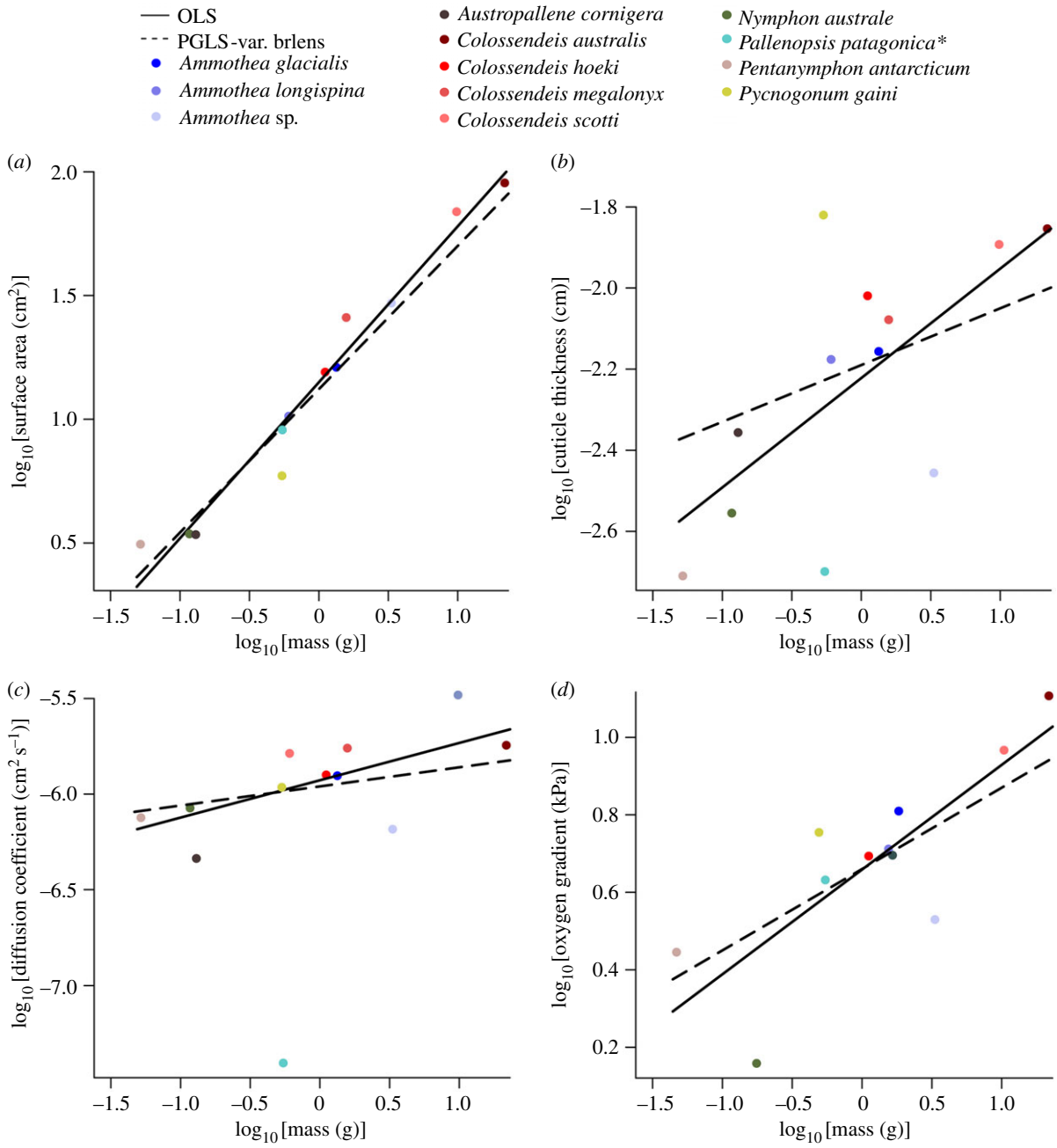

Figure 2. Scaling relationships for surface area ($N = 12$) (*a*), cuticle thickness ($N = 12$) (*b*), cuticle diffusion coefficient ($N = 11$) (*c*) and oxygen gradient ($N = 11$) (*d*) to body mass in Antarctic sea spiders. Lines indicate fits using OLS and PGLS-var. brlens regression. See table 1 for scaling coefficients, and the data used are listed in electronic supplementary material, tables S1–S3. **Pallenopsis patagonica* appears to be an outlier and was not used in calculating the diffusion coefficient scaling relationship.

gradient (ΔPO_2), we calculated flux (J) with equation (1.3). The capacitance coefficient of seawater (β) was taken from Dejours [7] based on ambient water temperatures (approximately -1°C).

(g) Statistical analysis

To analyse scaling relationships, we $\log_{10}$-transformed the data and then fitted ordinary least square models (OLS) to each respiratory variable (surface area, cuticle thickness, diffusion coefficient, oxygen gradient, flux, oxygen consumption and leg span) versus body mass. For most species, we took the average measurements from 2 to 11 individuals, which varied within each species and measurement (electronic supplementary material, tables S1–S3). However, we had only one individual of *Austropallene cornigera* and *Colossendeis australis*. All statistical analyses were carried out in R (v. 3.3.0) [26].

In comparative studies, closely related species tend to be similar because they share relatively recent common ancestry [31]. To account for this possibility, we conducted multiple phylogenetic general least square (PGLS) models using a tree built with mitochondrial cytochrome *c* oxidase (CO1) sequences collected from the samples used in this study. The tree was constructed using a maximum-likelihood approach in PAUP* (v4.0) [32]. The tree was constructed using the best model of molecular evolution selected by ModelTest (v3.7) [33] using Akaike information criteria. The best fit model was GTR + I + G. The tree was estimated using a heuristic search with the tree bisection reconnection algorithm for five replicate starting trees constructed by random sequence addition, and node robustness was estimated after 100 bootstrap replicates (electronic supplementary material, figure S2*a*). The topology of this tree was different from other published pycnogonid phylogenies [34]. Therefore, owing to limited taxonomic sampling in our dataset, we also created a second tree by constraining the topology at the family level to match the family topology of Arango & Wheeler [34] (electronic supplementary material, figure S2*b*). Their tree was built using six different

nuclear or mitochondria genes and included 63 species of Pycnogonida from all extant families. After constraining the topology of the tree in this manner, the branch lengths were left to vary based on our CO1 data. Because of our low taxon sampling and the associated uncertainty in branch lengths of a single gene tree, we bracketed our hypotheses by comparing our data based on a star phylogeny (OLS), an unconstrained phylogeny built with our CO1 data (PGLS-mtCO1), a constrained phylogeny where branch lengths were free to vary based on our CO1 data (PGLS-var. brlens) and a constrained phylogeny using equal branch lengths (i.e. setting branch lengths to one) (PGLS-equal brlens) which accounts for branching patterns among taxa but not branch lengths [32].

Phylogenetic generalized least-squares models were conducted using all three types of phylogenetic trees using the R package 'ape' (v3.5) [35,36]. In each case, we assumed a Brownian motion model of trait evolution [31], which was the same model Gillooly *et al*. used on similar trait data [8]. As in the OLS model described above, we used $\log_{10}$-transformed data and took species averages to fit each PGLS model.

We tested for phylogenetic signal using Pagel's lambda [37,38]. Estimates of lambda for the respiratory variables spanned from 0 (no phylogenetic signal) to 1 (strong phylogenetic signal). Log-likelihood tests showed that the lambdas for only two of the variables, cuticle thickness and flux, were significantly different from 0, but these two variables were not significant across all types of PGLS analyses (electronic supplementary material, table S4). After applying a Bonferroni correction to account for multiple comparisons within each variable ($\alpha = 0.05/3 = 0.017$), however, no value of lambda differed significantly from 0. Clearly, these analyses for phylogenetic signal are limited by taxonomic sampling, which may prevent us from identifying a signal even if it is present. In general, studies with more than 20 sampled taxa can detect phylogenetic signals if they are present, whereas those with fewer than 20 sampled taxa have substantially less power [39]. On the basis of the lack of almost any detectable phylogenetic signal, only the OLS results were discussed.

3. Results and discussion

In vertebrates, surface area and barrier thickness alone constrain oxygen flux (electronic supplementary material, figure S1*a*) [8]. Here, our results (table 1, figure 2*a–d*) indicate that surface area did not scale as high in Antarctic sea spiders as it does in vertebrates (0.63, figure 2*a*, and 0.89, respectively), but barrier thickness scaled higher in Antarctic sea spiders than in vertebrates (0.27, figure 2*b*, and 0.1, respectively) [8]. These differences probably result from the dual roles of the cuticle in both gas exchange and structural support. Furthermore, the combined scaling of surface area and cuticle thickness (i.e. $0.63 - 0.27 = 0.36$) does not scale high enough to meet the metabolic demands of sea spiders (0.8). To offset this disparity, both the effective cuticular diffusion coefficient and the oxygen gradient scaled positively with body size (0.2, figure 2*c*, and 0.27, figure 2*d*, respectively). The combined scaling of the diffusion coefficient, oxygen gradient, surface area, and barrier thickness give an estimate of flux scaling (i.e. $0.63 - 0.27 + 0.2 + 0.27 = 0.83$) that matches metabolic scaling very closely (0.8, figure 3). In contrast to vertebrates, therefore, in sea spiders, which rely on cutaneous respiration, all components of Fick's Law (except for β, because it is governed by physical properties) increase with body size (electronic supplementary material, figure S1*d*).

Like the scaling coefficients, the intercepts of estimated fluxes (from the Fick analysis) and of metabolic rate were quite similar (−3.71 and −3.96, respectively, with overlapping

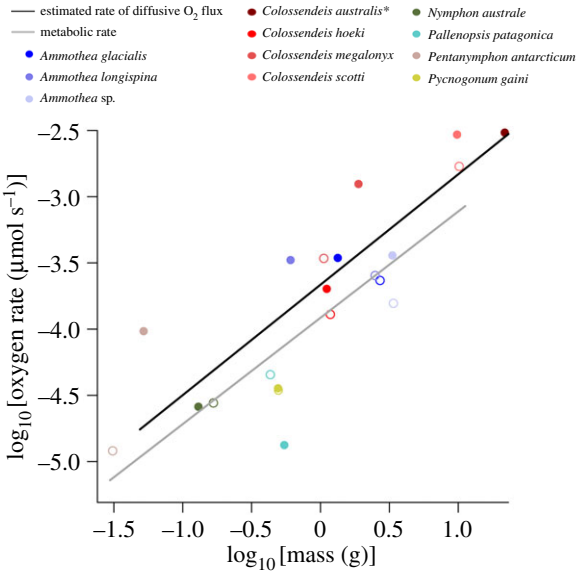

Figure 3. Scaling relationship for estimated rate of diffusive oxygen flux and metabolic rate to body mass in Antarctic sea spiders. The estimated rates of diffusive oxygen flux for each species are indicated by solid circles ($N = 11$) while the metabolic rate values are indicated by open circles ($N = 10$). Lines were fitted using OLS regression. See table 1 for scaling coefficients, and the data used are in electronic supplementary material, tables S1–S3. *We did not get metabolic data on *Colossendeis australis*.

confidence intervals). This close match means that our measurements and analyses account for all of the major processes contributing to metabolic fluxes of oxygen.

Two of the four tunable variables of Fick's law (equation (1.3)) cannot continue increasing indefinitely and so impose upper limits on body size: the cuticular diffusion coefficient (D_c) and the oxygen gradient across the cuticle (ΔPO_2). The cuticular diffusion coefficient rises with cuticular porosity, but it obviously cannot rise above some upper limit (e.g. 100% porosity would mean that the cuticle did not exist). Davenport *et al*. [23] calculated the porosity of one large Antarctic species (*Decalopoda australis*) to be about 35%. Here, as a conservative estimate, we estimated maximum porosity as 50%, which would give an effective diffusion coefficient of approximately half the diffusion coefficient of oxygen in seawater (5×10^{-6} cm^2 s^{-1}), assuming that the material within the pores does not significantly slow rates of diffusion. Together with the remaining scaling coefficients (table 1), this value indicates that sea spiders would approach this limit at approximately 1400 g (figure 4*a*). The scaling of the oxygen gradient also imposes limits. Physically, internal PO_2 cannot go below 0 kPa (gradient of approx. 21 kPa). Projecting out to larger body sizes (table 1) shows that sea spiders hit this limit at approximately 300 g (figure 4*b*), which means that the oxygen gradient should limit large size substantially sooner than should cuticle porosity. The largest sea spider (*Colossendeis colossea*) ever reported had a leg span somewhat larger than 70 cm but no body mass was given [5]. Using our scaling coefficients for leg span (table 1), a 70 cm sea spider has a projected body size of approximately 300 g (electronic supplementary material, figure S3), right at the size limit predicted by the scaling of the oxygen gradient. This analysis suggests that evolving larger size would require evolutionary innovations in the mechanisms for obtaining and distributing oxygen. For example, other groups of large-bodied marine invertebrates, such as

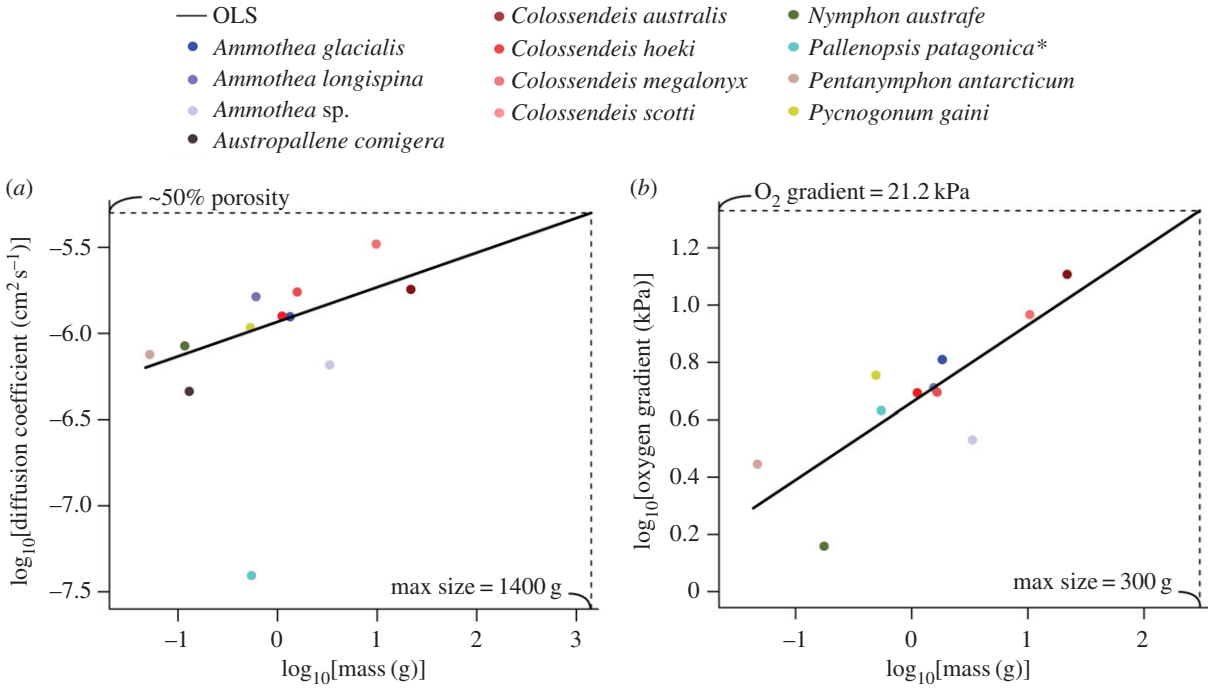

Figure 4. Upper limits to body size estimated from the diffusion coefficient ($N = 11$) (*a*) and oxygen gradient ($N = 11$) (*b*). Upper limits were found by extrapolating OLS regression line out to the point where the line intersected the estimated *y*-values. See table 1 for scaling coefficients. See text for details. **Pallenopsis patagonica* appears to be an outlier and was not used in calculating the upper limits to body size using the diffusion coefficient scaling relationship.

other groups of large arthropods (e.g. crustaceans), evade respiratory constraints by using both respiratory pigments and strong heart-driven flows of haemolymph [9]. Sea spiders drive circulatory flows with both their hearts and guts [40]. In addition, they are known to transcribe the genes for respiratory pigments (i.e. haemocyanin) [41], but no proteins have yet been detected in the haemolymph [42].

An obvious alternative path to balancing the oxygen budget would be to have thinner or more porous cuticle. One outlier in our data suggests that one species has done so. *Pallenopsis patagonica* has very low porosity (figure 2*c*) but also very thin cuticle for its body size (figure 2*b*). Perhaps its ecology protects it from strong external forces. We often found this species clinging to hydroids rather than walking freely on the benthos. We hypothesize that there is a trade-off between the ability of sea spiders to get oxygen and their ability to resist external forces. Extremely thin cuticle may buckle as the animal walks around, while cuticle constructed of more than half pores may collapse due to external forces. Alternatively, *Colossendeis* spp. have proportionally thick and porous cuticle for their body sizes (figure 2*b*,*c*). Individuals of these species were often found freely moving along the benthos, actively foraging. To quantify this trade-off, future studies should measure the mechanical strength of the cuticle with different levels of porosity. For example, some deep-sea species also grow to large sizes [5] but live in an environment with proportionately less oxygen. These species may also experience lower external forces (such as strong currents), which may allow them to evolve relatively thin, porous cuticles without risking breakage.

Body size profoundly alters both the demand of organisms for oxygen and the challenges and possible evolutionary solutions to obtaining it. Gillooly *et al*. [8] showed, in vertebrates, that changes in respiratory surface area and thickness alone are sufficient to balance the oxygen budget across body sizes. Our study, of sea spiders, provides a strikingly different picture: changes in body size lead to the simultaneous co-adjustment of four of the underlying Fick variables, not just surface area and cuticular thickness. Our result suggests that the evolutionary opportunities available to, and constraints operating on, respiratory systems across body sizes change in important ways among groups with different fundamental body plans. Moreover, alternative evolutionary trajectories among different high-level taxonomic groups (classes, phyla) probably play important roles in generating different upper limits to body size among groups.

Data accessibility. This article has no additional data.

Authors' contributions. S.J.L., A.L.M., B.W.T. and H.A.W. designed the experiments. S.J.L., C.M.S., A.L.M. and H.A.W. carried them out. S.J.L., A.L.M. and C.P.A. performed phylogenetic analyses. S.J.L., A.L.M. and H.A.W. wrote the manuscript. All authors gave final approval for manuscript.

Competing interests. We have no competing interests.

Funding. Funding was provided by NSF grant PLR-1341485 to H.A.W. and B.W.T. and PLR-1341476 to A.L.M.

Acknowledgements. We thank the staff and directors of McMurdo Station for technical and field support. Special thanks to Rob Robbins, Steve Rupp and Tim Dwyer for SCUBA support. We also thank Peter Marko, Michael Wallstrom, and Floyd Reed, Sachie Etherington, and the entire class of BIOL 375L from fall 2016 at the University of Hawai'i at Manoa for their contributions to the barcoding effort.

References

1. West GB, Brown JH, Enquist BJ. 1997 A general model for the origin of allometric scaling laws in biology. *Science* **276**, 122–126. (doi:10.1126/science.276.5309.122)

2. West GB, Brown JH. 2005 The origin of allometric scaling laws in biology from genomes to

ecosystems: towards a quantitative unifying theory of biological structure and organization. *J. Exp. Biol.* **208**, 1575–1592. (doi:10.1242/jeb.01589)

3. Banavar JR, Damuth J, Maritan A, Rinaldo A. 2002 Supply-demand balance and metabolic scaling. *Proc. Natl Acad. Sci. USA* **99**, 10 506–10 509. (doi:10.1073/pnas.162216899)
4. Fick A. 1855 Ueber diffusion. *Ann. Phys.* **170**, 59–86. (doi:10.1002/andp.18551700105)
5. Arnaud F, Bamber RN. 1987 The biology of Pycnogonida. *Adv. Mar. Biol.* **24**, 1–96.
6. Maina JN, West JB. 2005 Thin and strong! The bioengineering dilemma in the structural and functional design of the blood-gas barrier. *Physiol. Rev.* **85**, 811–844. (doi:10.1152/physrev.00022.2004)
7. Dejours P. 1981 *Principles of comparative respiratory physiology*, p. 265. Amsterdam, The Netherlands: Elsevier/North-Holland Biomedical Press.
8. Gillooly JF, Gomez JP, Mavrodiev EV, Rong Y, McLamore ES. 2016 Body mass scaling of passive oxygen diffusion in endotherms and ectotherms. *Proc. Natl Acad. Sci USA* **113**, 5340–5345. (doi:10.1073/pnas.1519617113)
9. Schmidt-Nielson K. 1984 *Scaling: why is animal size so important?* pp 241. Cambridge, UK: Cambridge University Press.
10. Mortola JP. 2015 Generalities of gas diffusion applied to the vertebrate blood–gas barrier. In *The vertebrate blood–gas barrier in health and disease*, (ed. AN Makanya), pp. 1–14. New York, NY: Springer.
11. Dawson TH. 2005 Modeling of vascular networks. *J. Exp. Biol.* **208**, 1687–1694. (doi:10.1242/jeb.01622)
12. Weibel ER, Taylor CR, Gehr P, Hoppeler H, Mathieu O, Maloiy GMO. 1981 Design of the mammalian respiratory system. IX. Functional and structural limits for oxygen flow. *Respir. Physiol.* **44**, 151–164. (doi:10.1016/0034-5687(81)90081-5)
13. Feder ME, Burggren WW. 1985 Skin breathing in vertebrates. *Sci. Am.* **253**, 126–142. (doi:10.1038/scientificamerican1185-126)
14. Graham JB. 1988 Ecological and evolutionary aspects of integumentary respiration: body size, diffusion, and the Invertebrata. *Am. Zool.* **28**, 1031–1045. (doi:10.1093/icb/28.3.1031)
15. Carey C. 1980 Introduction to the symposium: physiology of the avian egg. *Am. Zool.* **20**, 325–327. (doi:10.1093/icb/20.2.325)
16. Clarke BT. 1997 The natural history of amphibian skin secretions, their normal functioning and potential medical applications. *Biol. Rev. Camb. Philos. Soc.* **72**, 365–379. (doi:10.1017/S0006323197005045)
17. Rollins-Smith LA, Reinert LK, O'Leary CJ, Houston LE, Woodhams DC. 2005 Antimicrobial peptide defenses in amphibian skin. *Integr. Comp. Biol.* **45**, 137–142. (doi:10.1093/icb/45.1.137)
18. Kern MD, Ferguson MWJ. 1997 Gas permeability of American alligator eggs and its anatomical basis. *Physiol. Zool.* **70**, 530–546. (doi:10.1086/515860)
19. Woods HA, Bonnecaze RT, Zrubek B. 2005 Oxygen and water flux across eggshells of *Manduca sexta*. *J. Exp. Biol.* **208**, 1297–1308. (doi:10.1242/jeb.01525)
20. Ar A, Paganelli CV, Reeves RB, Greene DG, Rahn H. 1974 The avian egg: water vapor conductance, shell thickness, and functional pore area. *Condor* **76**, 153–158. (doi:10.2307/1366725)
21. Paganelli CV, Olzowka A, Ar A. 1974 The avian egg: surface area, volume, and density. *Condor* **76**, 319–325. (doi:10.2307/1366345)
22. Ar A, Rahn H. 1985 Pores in avian eggshells: gas conductance, gas exchange and embryonic growth rate. *Respir. Physiol.* **61**, 1–20. (doi:10.1016/0034-5687(85)90024-6)
23. Davenport J, Blackstock N, Davies A, Yarrington M. 1987 Observations on the physiology and integumentary structure of the Antarctic pycnogonid *Decolopoda australis*. *J. Zool.* **22**, 451–465. (doi:10.1111/j.1469-7998.1987.tb01545.x)
24. Woods HA, Moran AL, Arango CP, Mullen L, Shields C. 2009 Oxygen hypothesis of polar gigantism not supported by performance of Antarctic pycnogonids in hypoxia. *Proc. Biol. Sci.* **276**, 1069–1075. (doi:10.1098/rspb.2008.1489)
25. Geller J, Meyer C, Parker M, Hawk H.. 2013 Redesign of PCR primers for mitochondrial cytochrome c oxidase subunit I for marine invertebrates and application in all-taxa biotic surveys. *Mol. Ecol. Res.* **13**, 851–861. (doi:10.1111/1755-0998.12138)
26. R Core Team. 2016 *R: A language and environment for statistical computing*. Vienna, Austria: R Foundation for Statistical Computing.
27. Rasband WS. 2014 ImageJ [Online]. U.S. National Institutes of Health, Bethesda, MD. See http://imagej.nih.gov/ij/ [2015, June 1].
28. Key Jr MM, Knauff JB, Barnes DKA. 2013 Epizoic bryozoans on predatory pycnogonids from the South Orkney Islands, Antarctica: 'If you can't beat them, join them'. *Lect. Notes Earth Syst. Sci.* **143**, 137–153. (doi:10.1007/978-3-642-16411-8_10)
29. Woods HA, Moran AL. 2008 Oxygen profiles in egg masses predicted from a diffusion-reaction model. *J. Exp. Biol.* **211**, 790–797. (doi:10.1242/jeb.014613)
30. Crank J. 1975 *The mathematics of diffusion*, p. 414. 2nd edn. Oxford, UK: Oxford University Press.
31. Felsenstein J. 1985 Phylogenies and the comparative method. *Am. Nat.* **125**, 1–15. (doi:10.1086/284325)
32. Swofford DL. 2003 *PAUP* phylogenetic analysis using parsimony (* and other methods), version 4*. Sunderland, MA: Sinauer Associates.
33. Posada D, Crandall KA. 1998 ModelTest: testing the model of DNA substitution. *Bioinformatics* **14**, 817–818. (doi:10.1093/bioinformatics/14.9.817)
34. Arango CP, Wheeler WC. 2007 Phylogeny of the sea spiders (Arthropoda, Pycnogonida) based on the direct optimization of six loci and morphology. *Cladistics* **23**, 255–293. (doi:10.1111/j.1096-0031.2007.00143.x)
35. Pagel MD. 1992 A method for the analysis of comparative data. *J. Theor. Biol.* **156**, 431–442. (doi:10.1016/S0022-5193(05)80637-X)
36. Paradis E. 2012 *Analysis of phylogenetics and evolution with R*. New York, NY: Springer.
37. Pagel, MD. 1999 Inferring the historical patterns of biological evolution. *Nature* **401**, 877–884. (doi:10.1038/44766)
38. Revell, LJ. 2010 Phylogenetic signal and linear regression on species data. *Methods Ecol. Evol.* **1**, 319–329. (doi:10.1111/j.2041-210X.2010.00044.x)
39. Blomberg SP, Garland Jr T, Ives AR. 2003 Testing for phylogenetic signal in comparative data: behavioral traits are more labile. *Evolution* **57**, 717–745. (doi:10.1111/j.0014-3820.2003.tb00285.x)
40. Woods HA, Lane SJ, Shishido C, Tobalske BW, Arango CP, Moran AL. 2017 Respiratory gut peristalsis by sea spiders. *Curr. Biol.* **27**, R638–R639. (doi:10.1016/j.cub.2017.05.062)
41. Rehm P, Pick C, Borner J, Markl J, Burmester T. 2012 The diversity and evolution of chelicerate hemocyanins. *BMC Evol. Biol.* **12**, 19. (doi:10.1186/1471-2148-12-19)
42. Markl J. 1986 Evolution and function of structurally diverse subunits in the respiratory protein hemocyanin from arthropods. *Biol. Bull.* **171**, 90–115. (doi:10.2307/1541909)